LETTERS
https://doi.org/10.1038/s41558-019-0665-8
nature climate change

Increased global nitrous oxide emissions from streams and rivers in the Anthropocene

Yuanzhi Yao[1], Hanqin Tian[1]*, Hao Shi[1], Shufen Pan[1], Rongting Xu[1], Naiqing Pan[1] and Josep G. Canadell[2]

Emissions of nitrous oxide (N_2O) from the world's river networks constitute a poorly constrained term in the global N_2O budget[1,2]. This N_2O component was previously estimated as indirect emissions from agricultural soils[3] with large uncertainties[4–10]. Here, we present an improved model representation of nitrogen and N_2O processes of the land–ocean aquatic continuum[11] constrained with an ensemble of 11 data products. The model–data framework provides a quantification for how changes in nitrogen inputs (fertilizer, deposition and manure), climate and atmospheric CO_2 concentration, and terrestrial processes have affected the N_2O emissions from the world's streams and rivers during 1900–2016. The results show a fourfold increase of global riverine N_2O emissions from 70.4 ± 15.4 Gg N_2O-N yr^{-1} in 1900 to 291.3 ± 58.6 Gg N_2O-N yr^{-1} in 2016, although the N_2O emissions started to decline after the early 2000s. The small rivers in headwater zones (lower than fourth-order streams) contributed up to 85% of global riverine N_2O emissions. Nitrogen loads on headwater streams and groundwater from human activities, primarily agricultural nitrogen applications, play an important role in the increase of global riverine N_2O emissions.

Many studies have estimated nitrous oxide (N_2O) emissions from inland waters as the product of dissolved inorganic nitrogen by applying a laboratory-measured emission factor[4,5]. Emission factors (the ratio of N_2O emissions to riverine inorganic nitrogen) are determined from field experiments or observations, which limit their use at a large spatial-scale and a long time-scale in which land and river conditions show high heterogeneity. That is, it would be difficult to obtain emission factors at the large required spatiotemporal scales. Currently, the wide range of emission factors available results in a wide spread of existing estimates of riverine N_2O emissions[4–10] from 0.03 to 2.0 Tg N_2O-N yr^{-1}. Using laboratory-measured emission factors also ignores the transport process of N_2O in aquatic ecosystems. As a result of this limited knowledge, global land and earth system models are lacking the representation of lateral fluxes and processes over continents and from continents to oceans[12,13]. To determine the global N_2O budget and properly attribute atmospheric changes to sources and sinks, it is important to understand and quantify riverine nitrogen exports and associated N_2O emissions through the land–ocean aquatic continuum.

Here, we developed a riverine N_2O model within the framework of the dynamic land ecosystem model[14] (DLEM; Supplementary Fig. 1a) by coupling a scale-adaptive hydrological scheme[15] and river biogeochemistry[16] to simulate the riverine fluxes of water, carbon and nitrogen and the resulting emissions of GHGs. The model can effectively address the small stream processes by incorporating the subgrid routine processes without conducting model simulation at fine resolution (Supplementary Fig. 1b). To quantify the influences of natural and human activities on riverine N_2O emissions, the model was driven by many factors including climate (shortwave radiation, precipitation, air temperature, maximum temperature and minimum temperature), land use and land cover, and nitrogen inputs (fertilizer, deposition, manure and sewage) from 1900 to 2016 (Supplementary Fig. 2). The simulated river discharges and nitrate (NO_3^-), ammonium (NH_4^+) and dissolved organic nitrogen concentrations were calibrated using observations from 50 large river basins across the globe (Supplementary Fig. 3). The simulated groundwater-dissolved N_2O concentration and riverine-dissolved N_2O concentration agreed well with observations both spatially and temporally (Supplementary Table 1 and Supplementary Figs. 4–6). To assess the uncertainty of riverine N_2O emissions, six datasets of N inputs and five estimates of river surface area (Methods and Supplementary Fig. 7) were used to drive the model. The average of the ensemble N_2O outputs was taken as the best estimation. Moreover, factorial experiments (Fig. 1b) were conducted to attribute the contribution of each factor (climate, CO_2, fertilizer, manure and N deposition) to riverine N_2O emissions (Supplementary Table 2).

We estimate that global riverine N_2O emissions increased from 70.4 ± 15.4 Gg N_2O-N yr^{-1} in 1900 to 291.3 ± 58.6 Gg N_2O-N yr^{-1} in 2016, at an average annual growth rate of 1.92 Gg N_2O-N yr^{-1} (trend 1 in Fig. 1a). The increasing trend was not monotonic and its evolution can be partitioned into the three periods 1900–1966, 1967–1996 and 1997–2016, according to the piecewise linear regression. During 1900–1966, the increasing growth rate was 1.02 Gg N_2O-N yr^{-1} ($P < 0.05$) primarily driven by multiple sources of N input (Fig. 1b). For example, in the 1950s manure contributed 39.9% (12.1 Gg N_2O-N yr^{-1}) to the global increase, with N deposition 23.6% (7.1 Gg N_2O-N yr^{-1}) and N fertilizer 25.5% (7.7 Gg N_2O-N yr^{-1}; Fig. 1b). During 1967–1996, the increasing growth rate accelerated to 4.57 Gg yr^{-1} due to the wide use of N fertilizer, which contributed 85.8% (121 Gg N_2O-N yr^{-1}) of the global increase during the 1990s. However, global riverine N_2O emissions started to decrease during 2010–2016 at a rate of 1.03 Gg N_2O-N yr^{-1}, partially due to decreased N fertilizer use as well as elevated CO_2-induced reduction in N_2O emissions (−17.5%, −24.6 Gg N_2O-N yr^{-1}). The CO_2 fertilization effect promotes increased plant growth at higher CO_2 concentrations and therefore locks more nitrogen into plant biomass[17].

The contribution of small rivers (lower than fourth-order streams) dominated global riverine N_2O emissions (Fig. 2). For example, in the 2000s, N_2O emissions from small rivers were

[1]International Center for Climate and Global Change Research, School of Forestry and Wildlife Sciences, Auburn University, Auburn, AL, USA. [2]Global Carbon Project, CSIRO Oceans and Atmosphere, Canberra, Australian Capital Territory, Australia. *e-mail: tianhan@auburn.edu

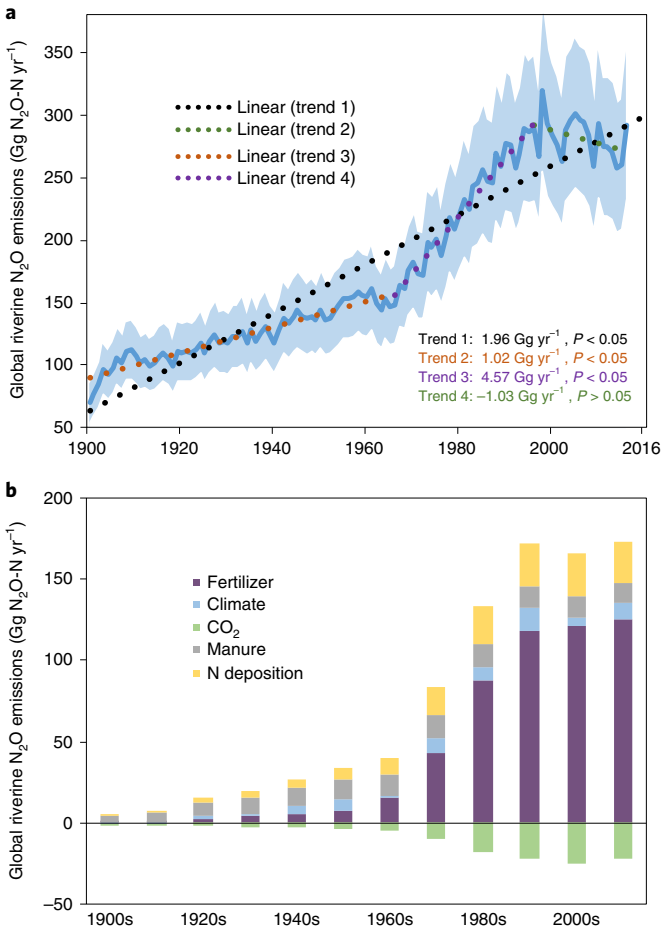

Fig. 1 | Temporal pattern of global riverine N_2O emission and factorial analysis from 1900 to 2016. a, Global riverine N_2O emissions from 1900 to 2016 with uncertainty ranges shaded in blue (±1 s.d.). **b**, The factorial contributions to global riverine N_2O emissions from the 1900s to the period 2007–2016.

241.4 ± 58.9 Gg N_2O-N yr^{-1} whereas emissions from high-order streams only were 42.5 ± 14.4 Gg N_2O-N yr^{-1} (Fig. 2). Groundwater processes, which include the lateral transport of groundwater from the soil root zone and biogeochemical processes occurring in the hyporheic zone (beneath the stream bed where groundwater and stream water interact), were the major source of N_2O and produced on average 391 ± 76.6 Gg N_2O-N yr^{-1} during the 2000s. In contrast, during the same time period, water column processes within small stream and large rivers accounted for an average of 4.1 ± 2.1 and 42.4 ± 19.8 Gg N_2O-N yr^{-1}, respectively (Fig. 2).

At the global scale, the major riverine N_2O sources were in tropical regions and intensively cultivated croplands, such as the central United States, Europe, India, Southeast Asia and east China. The latitudinal pattern showed that temperate regions replaced tropical regions as the areas with the highest intensity of riverine N_2O emissions in the 2000s (Fig. 3). Yet we note that in some high-latitude and arid regions, rivers acted as a sink for N_2O, consistent with the experimental evidience[6,18] (Fig. 3). This may be due to relatively low terrestrial-N inputs and the resultant low dissolved N_2O production in groundwater and surface water.

We divided the global land area into ten unique regions according to their geographical and socioeconomic characteristics (Fig. 4) and 45 regions based on the distribution of coastal lines (Supplementary Table 3 and Supplementary Fig. 9). Before the 1980s, riverine N_2O emissions showed considerable increases in all regions (Fig. 4). Owing to intensive N fertilizer inputs after the 1980s, rapid increase in riverine N_2O emissions occurred in the three regions of Asia (45.65 Gg N_2O-N yr^{-1} in East Asia, 22.69 Gg N_2O-N yr^{-1} in South Asia and 4.29 Gg N_2O-N yr^{-1} in Southeast Asia in the 1990s; Supplementary Fig. 10). Since the 1990s, the riverine N_2O emissions in developed regions (North America, Europe, Oceania and the Middle East) gradually reached a peak and then began to decrease, mainly due to reduced fertilizer use and the CO_2 fertilization effect on plant growth. In addition, developing regions, Africa and Central America also contributed to the decrease in global riverine N_2O emissions since 1996, as a result of the effects of climate and elevated CO_2 (Supplementary Fig. 10).

Our approach is capable of estimating riverine N_2O emissions from both small streams and high-order rivers at fine spatial and temporal resolutions, thus overcoming the limitations of the emission factor approach. The results reveal the disproportionately large contribution of small rivers to global riverine N_2O emissions, as already hinted by several regional studies[19,20]. Smaller streams experience more hyporheic exchange, which facilitates increased N_2O production due to the large biochemically reactive surface area of the hyporheic zone. Compared to the high-order streams, low-order streams directly fed by hyporheic exchanges[21], have higher dissolved N_2O concentrations, steeper channel slopes and faster flow velocities, which all contribute to higher gas exchange rates[20]. The dominant role of small rivers at the global scale was not recognized for a long time because they are not consistently gauged for discharge and it is difficult to directly measure their surface area[22].

We tested how well our model predicted riverine N_2O emissions by separately comparing the contribution of headwater streams and high-order streams with previous studies (Supplementary Table 4). Beaulieu et al.[6] applied emission factors observed in headwater streams to the whole riverine system and obtained an estimate of 680 Gg N_2O-N yr^{-1}, which overestimated N_2O emissions from the high-order steams due to their sampling sites being mostly selected from headwater streams[9]. Although the value reported by Beaulieu et al.[6] is an overestimate, we can use it to back-calculate headwater emissions for comparison to our modelled value. Considering that the water surface area of headwater streams accounts for 44.4% of the global active river surface area[23], the riverine N_2O emissions from headwater streams can be roughly estimated (680 Gg N_2O-N $yr^{-1} \times 44.4\%$) at about 301.8 Gg N_2O-N yr^{-1}, which is comparable to our estimate (241.4 ± 58.9 Gg N_2O-N yr^{-1}). Similarly, we can derive the contribution of high-order streams using global riverine N_2O emissions that used emission factors measured in high-order streams. Our estimate for large rivers (42.5 ± 14.4 Gg N_2O-N yr^{-1}) is comparable to other previous estimates (32 Gg N_2O-N yr^{-1} from ref. [9] and 39.2–49.4 Gg N_2O-N yr^{-1} from ref. [8]).

It is worth noting that most of the dissolved N_2O in the water column was from N_2O-supersaturated groundwater (Fig. 2), addressing the balance of N_2O emissions in excess of that produced via direct denitrification[21]. This phenomena could be explained by the long residence time[21] of subsurface transport, which provides enough time for denitrification to convert NO_3^- into N_2O and nitrogen gas. The long residence time induces a high rate of leached nitrogen accumulating in the groundwater pool and resulting in high N_2O concentration. Additionally, the low oxygen level[24] below the water table provides favourable conditions for the production of N_2O via denitrification, which in turn produced more N_2O in groundwater.

Anthropogenic N inputs and cropland expansions could explain most of the increase in the groundwater N_2O concentration and global riverine N_2O emissions[25]. Among regions, the substantial increase of riverine N_2O emissions in China, South Asia and Southeast Asia since the 1980s (Fig. 4) is due to the rapid growth in population, which has boosted the demand for food and

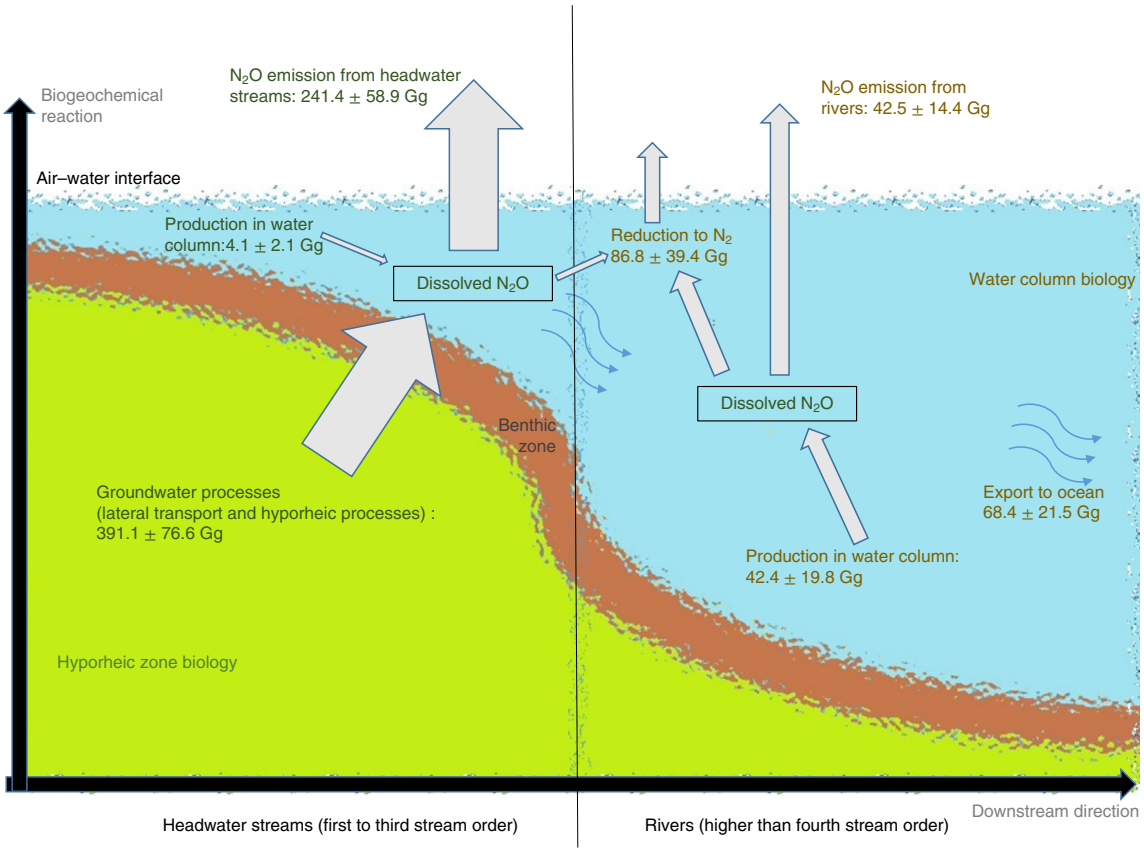

Fig. 2 | Global annual mean riverine N_2O fluxes during the 2000s estimated by DLEM. All the arrows denote N_2O fluxes. The left side of the figure depicts biogeochemical processes in the headwater zone simulated in subgrid routine processes at a resolution of 0.5° × 0.5°. The dissolved N_2O of headwater zone exports to downstream river channels (right side) were simulated through the DLEM cell-to-cell routine processes. The benthic zone indicates the sediment surface and its subsurface layers located at the lower end of the waterbodies.

industrial supplies, and has stimulated the heavy use of N fertilizer and manure. For example, China consumed about 30% of global total nitrogen fertilizer during 2007–2016 with less than 7% of the global cropland area[26]. In contrast, the CO_2 fertilization effect is the main reason for the decrease in global riverine N_2O emissions since the early 2000s (Fig. 1b). Increased vegetation growth requires more uptake of NO_3^-, which leads to less NO_3^--N being exported into rivers, and therefore decreased N_2O production through denitrification[27]. However, the magnitude of CO_2 fertilization effect on plant growth and nitrogen cycling remains largely uncertain[28].

Our model unveils the global spatiotemporal pattern of riverine N_2O emissions and the underlying governing factors of emissions. The results showing asynchronous temporal changes in N_2O emissions and NO_3^- concentrations (Supplementary Figs. 6 and 8) in high-order streams suggest that it is not appropriate to use NO_3^- as an instantaneous predictor for riverine N_2O fluxes. We found that the temporal N_2O production was regulated by water temperature[25], as well as the riverine NO_3^- content that is greatly affected by riverine transport with limited removal rates[29].

Our study highlights the importance of surface and subsurface processes in N_2O emissions from the world's river networks. We show that large N_2O emissions from headwater or small rivers have been ignored or underestimated in recent estimates of riverine N_2O emissions[8,9]. It is known that applying a constant emission factor measured from headwater streams leads to overestimated N_2O emissions from the world's rivers[8]. To better estimate N_2O emissions from the world's river networks, models need to improve the representation of surface and subsurface hydrological and biogeochemical processes; measurements and driving data also need to improve. In particular, model parameters were the largest source of uncertainty, followed by river surface area and nitrogen inputs (Supplementary Fig. 7). A rainfall event can increase the surface area of the first-order streams greatly but the high flow velocities make surface area prediction difficult[22]. Gas exchange rates also show large variations by streams which requires further investigation[30]. We simulated the N_2O production from nitrification and denitrification using a Q_{10}-based empirical method, in which water temperature is the only determinant (the first-order mechanism). Although some deficits exist in this method to explicitly account for other critical factors, such as carbon availability, microbe activity and the level of dissolved oxygen (Supplementary Fig. 7), the parameterization of nitrification and denitrification rates at the reference temperature does implicitly consider impacts of other factors. Moreover, the method is further validated by this study (Supplementary Table 1)[25]. Currently, the process-based subsurface hydrodynamic model requires variables such as thickness or extent of the hyporheic zone, hyporheic denitrification rate[21]. However, these variables remain highly uncertain due to the lack of field measurements globally. Therefore, the rigorous interaction between process-based modelling and field experimentation will be essential to reduce estimate uncertainty in the lateral N_2O emission for closing the global N_2O budget.

Global riverine N_2O emissions, as one component of the inland water systems (lake, reservoir, river and estuary) account for about 3% of global terrestrial N_2O emission[1] but the increasing rate of these riverine emissions is three times faster than the terrestrial

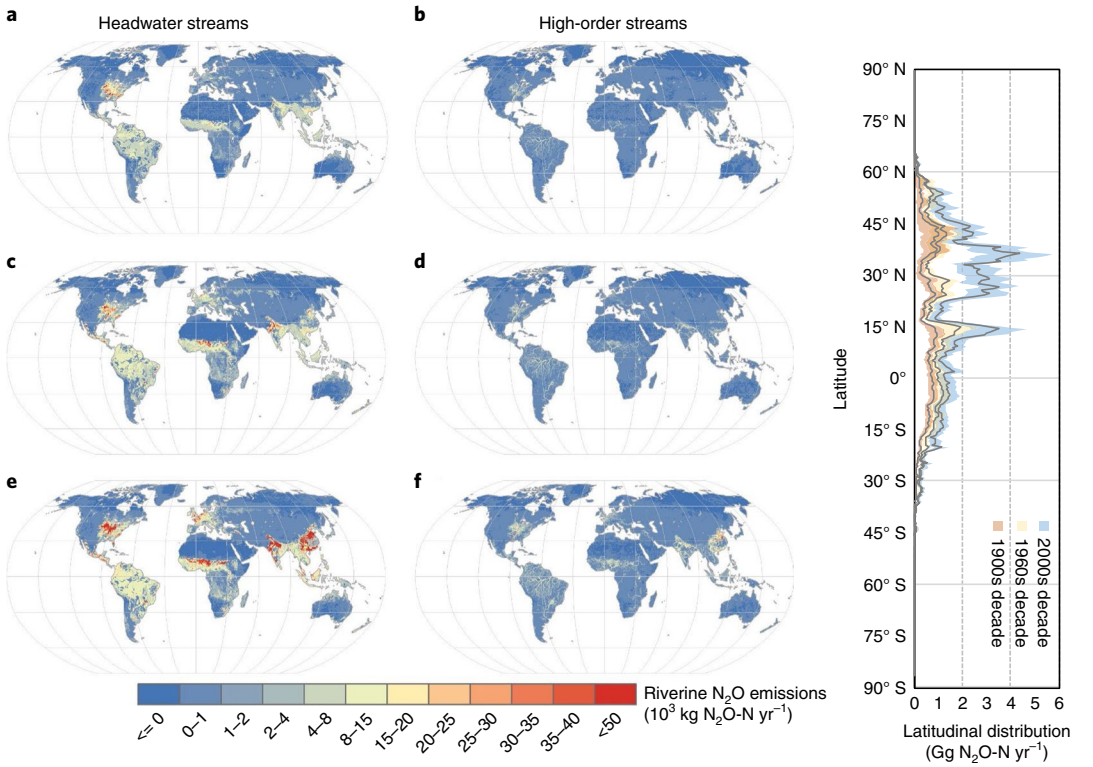

Fig. 3 | The spatial distribution of modelled annual total N_2O emission at a resolution of 0.5° × 0.5°. a,**c**,**e**, The riverine N_2O emission from headwater streams (lower than fourth stream orders) during the 1900s (**a**), the 1960s (**c**) and the 2000s (**e**). **b**,**d**,**f**, The riverine N_2O emission from high-order rivers (higher than fourth stream order) during the 1900s (**b**), the 1960s (**d**) and the 2000s (**f**). The right panel shows the latitudinal distribution of riverine N_2O emissions during the 1900s, the 1960s and the 2000s. The uncertainty range is ±1s.d. (the shaded area).

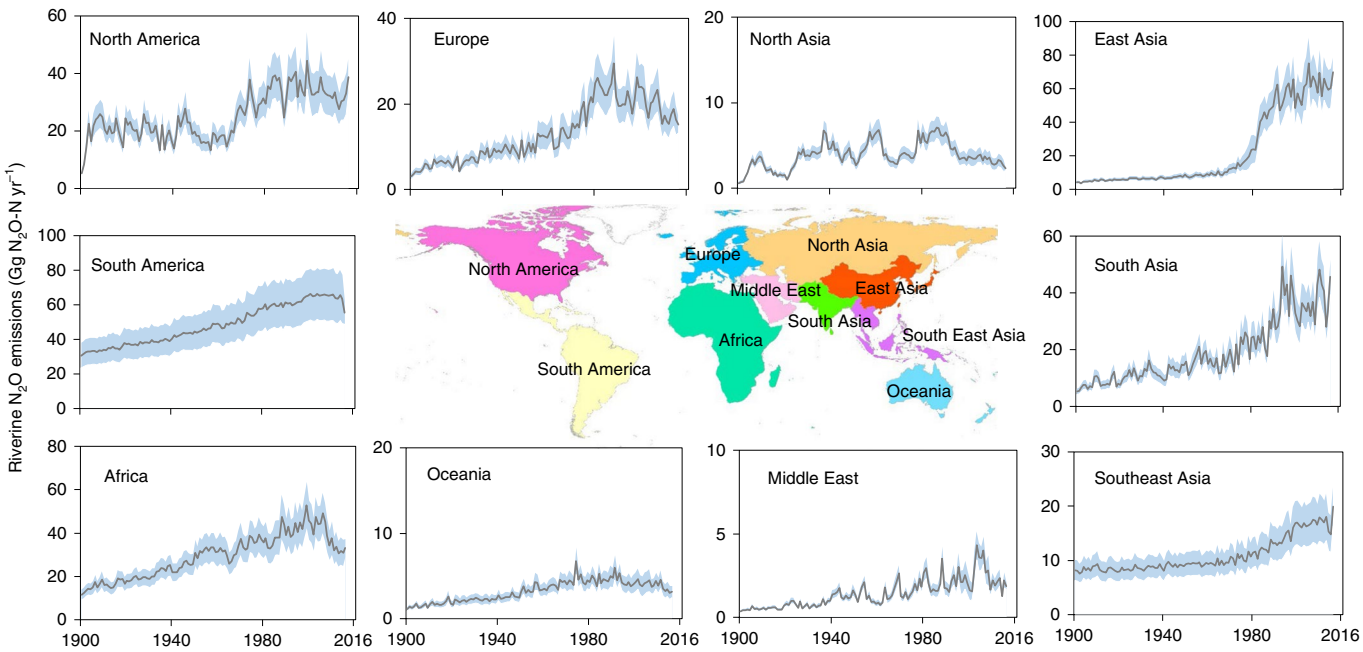

Fig. 4 | Interannual variations of riverine N_2O emissions in the ten regions from 1900 to 2016. The uncertainty range is ±1s.d. (the shaded area). Note that the vertical scales are different for subplots.

ones[13]. The improved knowledge of the quantities, distribution and hotspots of riverine N_2O emissions from this study can support the implementation of management strategies to increase crop nitrogen efficiency, thereby reducing nitrogen losses and their associated environmental impacts. Our study suggests that it is critical to reduce nitrogen loads into the headwater streams

that are closer to human activities. All GHG emission pathways consistent with the goals of the Paris Climate Agreement require large and sustained reductions on N_2O emissions, which in turn require improved quantification, process attribution and methodological transparency.

Online content

Any methods, additional references, Nature Research reporting summaries, source data, extended data, supplementary information, acknowledgements, peer review information; details of author contributions and competing interests; and statements of data and code availability are available at https://doi.org/10.1038/s41558-019-0665-8.

Received: 26 January 2019; Accepted: 19 November 2019;
Published online: 23 December 2019

References

1. Ciais, P. et al. in *Climate Change 2013: The Physical Science Basis* (eds Stocker, T. F. et al.) 465–570 (IPCC, Cambridge Univ. Press, 2014).
2. Tian, H. et al. The terrestrial biosphere as a net source of greenhouse gases to the atmosphere. *Nature* **531**, 225–228 (2016).
3. Davidson, E. A. & Kanter, D. Inventories and scenarios of nitrous oxide emissions. *Environ. Res. Lett.* **9**, 105012 (2014).
4. Seitzinger, S. P., Kroeze, C. & Styles, R. V. Global distribution of N_2O emissions from aquatic systems: natural emissions and anthropogenic effects. *Chemosphere-Glob. Change Sci.* **2**, 267–279 (2000).
5. Kroeze, C., Dumont, E. & Seitzinger, S. P. New estimates of global emissions of N_2O from rivers and estuaries. *Environ. Sci.* **2**, 159–165 (2005).
6. Beaulieu, J. J. et al. Nitrous oxide emission from denitrification in stream and river networks. *Proc. Natl Acad. Sci. USA* **108**, 214–219 (2011).
7. Kroeze, C. & Seitzinger, S. P. Nitrogen inputs to rivers, estuaries and continental shelves and related nitrous oxide emissions in 1990 and 2050: a global model. *Nutr. Cycl. Agroecosyst.* **52**, 195–212 (1998).
8. Maavara, T. et al. Nitrous oxide emissions from inland waters: are IPCC estimates too high? *Glob. Change Biol.* **25**, 473–488 (2018).
9. Hu, M., Chen, D. & Dahlgren, R. A. Modeling nitrous oxide emission from rivers: a global assessment. *Glob. Change Biol.* **22**, 3566–3582 (2016).
10. Reay, D. S. et al. Global agriculture and nitrous oxide emissions. *Nat. Clim. Change* **2**, 410 (2012).
11. Regnier, P. et al. Anthropogenic perturbation of the carbon fluxes from land to ocean. *Nat. Geosci.* **6**, 597 (2013).
12. Ciais, P. et al. The impact of lateral carbon fluxes on the European carbon balance. *Biogeosciences* **5**, 1259–1271 (2008).
13. Tian, H. et al. Global soil nitrous oxide emissions since the preindustrial era estimated by an ensemble of terrestrial biosphere models: magnitude, attribution, and uncertainty. *Glob. Change Biol.* **25**, 640–659 (2018).
14. Tian, H. et al. Anthropogenic and climatic influences on carbon fluxes from eastern North America to the Atlantic Ocean: a process-based modeling study. *J. Geophys. Res. Biogeosci.* **120**, 757–772 (2015).
15. Li, H.-Y. et al. Evaluating global streamflow simulations by a physically based routing model coupled with the community land model. *J. Hydrometeorol.* **16**, 948–971 (2015).
16. Yang, Q. et al. Increased nitrogen export from eastern North America to the Atlantic Ocean due to climatic and anthropogenic changes during 1901–2008. *J. Geophys. Res. Biogeosci.* **120**, 1046–1068 (2015).
17. Terrer, C. et al. Nitrogen and phosphorus constrain the CO_2 fertilization of global plant biomass. *Nat. Clim. Change* **9**, 684–689 (2019).
18. Soued, C., del Giorgio, P. A. & Maranger, R. Nitrous oxide sinks and emissions in boreal aquatic networks in Québec. *Nat. Geosci.* **9**, 116–120 (2016).
19. Turner, P. A. et al. Indirect nitrous oxide emissions from streams within the US Corn Belt scale with stream order. *Proc. Natl Acad. Sci. USA* **112**, 9839–9843 (2015).
20. Garnier, J. et al. Nitrous oxide (N_2O) in the Seine river and basin: observations and budgets. *Agric. Ecosyst. Environ.* **133**, 223–233 (2009).
21. Marzadri, A., Dee, M. M., Tonina, D., Bellin, A. & Tank, J. L. Role of surface and subsurface processes in scaling N_2O emissions along riverine networks. *Proc. Natl Acad. Sci. USA* **114**, 4330–4335 (2017).
22. Allen, G. H. et al. Similarity of stream width distributions across headwater systems. *Nat. Commun.* **9**, 610 (2018).
23. Raymond, P. A. et al. Global carbon dioxide emissions from inland waters. *Nature* **503**, 355–359 (2013).
24. Rosamond, M. S., Thuss, S. J. & Schiff, S. L. Dependence of riverine nitrous oxide emissions on dissolved oxygen levels. *Nat. Geosci.* **5**, 715–718 (2012).
25. Quick, A. M. et al. Nitrous oxide from streams and rivers: a review of primary biogeochemical pathways and environmental variables. *Earth-Sci. Rev.* **191**, 224–262 (2019).
26. *FAOSTAT Database* (FAO, 2018).
27. Kanter, D. R., Zhang, X., Mauzerall, D. L., Malyshev, S. & Shevliakova, E. The importance of climate change and nitrogen use efficiency for future nitrous oxide emissions from agriculture. *Environ. Res. Lett.* **11**, 094003 (2016).
28. Liu, Y. et al. Field-experiment constraints on the enhancement of the terrestrial carbon sink by CO_2 fertilization. *Nat. Geosci.* **12**, 809–814 (2019).
29. Loken, L. C. et al. Limited nitrate retention capacity in the Upper Mississippi River. *Environ. Res. Lett.* **13**, 074030 (2018).
30. Ulseth, A. J. et al. Distinct air–water gas exchange regimes in low- and high-energy streams. *Nat. Geosci.* **12**, 259 (2019).

Methods

We collected site-level observations of dissolved N_2O concentration, riverine N_2O flux and groundwater N_2O concentration from literature, to calibrate and validate our riverine N_2O model within the DLEM framework (Supplementary Information). Meanwhile, six collected datasets of nitrogen input and an estimate of river water surface area were used to evaluate the input data-induced uncertainties in riverine N_2O emissions. The detailed information on the model and input data are given as follows.

The model. The DLEM is a fully distributed, process-based land surface model which couples the major land hydrological processes, plant physiology, soil biogeochemistry and riverine routine processes[14] (Supplementary Fig. 1). The DLEM explicitly simulates the carbon, nitrogen and water fluxes between plants, soil and atmosphere driven by climate, atmospheric CO_2, nitrogen deposition, land use and land cover, N fertilizer use, irrigation and other management practices. Meanwhile, the surface and drainage runoff and nitrogen load from DLEM are used as the input of the riverine model[16]. The simulated nitrogen loads include nitrate (NO_3^-), ammonium (NH_4^+) and dissolved organic nitrogen.

The DLEM riverine model calculates river routing and the biogeochemical processes in the aquatic ecosystems. The mineralization of dissolved organic nitrogen to NH_4^+ is mainly controlled by water temperature, while NH_4^+ nitrification and NO_3^- denitrification are primarily regulated by water temperature and flow velocity. Detailed descriptions of DLEM aquatic biogeochemical processes can be found in refs. [14] and [16]. In this study, we improved the DLEM aquatic model through adopting a scale-adaptive river routine approach[15] (Supplementary Information), to quantify the physical and biogeochemical processes in small streams, which usually cannot be accounted for in most regional and global modelling research[12,13]. In addition, a riverine N_2O model (Supplementary Information) was developed for simulating N_2O emissions from river channels.

Data sources. The model forcing consists of land use/land cover change, climate variables, atmospheric CO_2 and N_2O concentrations, atmospheric N deposition, nitrogen fertilizer and manure nitrogen applications (Supplementary Fig. 2).

The annual land use/land cover change data were derived from a potential natural vegetation map (synergetic land cover product[31]) and a prescribed cropland area dataset from the history database of the global environment v.3.2 (HYDE 3.2, ftp://ftp.pbl.nl/hyde/). The daily climate variables (precipitation, mean temperature, maximum temperature, minimum temperature and shortwave radiation) were obtained from the CRU–NCEP dataset (https://vesg.ipsl.upmc.fr) for 1900–2016. Annual atmospheric CO_2 concentration from 1900 to 2015 was obtained from the NOAA GLOBALVIEW-CO_2 dataset (https://www.esrl.noaa.gov). Long-term atmospheric N_2O concentration was obtained from the AGAGE dataset (https://agage.mit.edu/data/agage-data).

Model simulations were driven by multiple data sources of N deposition and N fertilizer use, including two datasets of N deposition at a resolution of 0.5°×0.5° from the atmospheric chemistry and climate model intercomparison project (ACCMIP)[32] and chemistry–climate model initiative (CCMI) models[33]. Three datasets of agricultural N fertilizer use were obtained from refs. [34–36].A spatially explicit dataset of manure N application on global croplands developed by Zhang et al.[37] was also used to drive DLEM. Additional detailed information about nitrogen inputs can be found in Supplementary information and other published documents[32–36].

The ACCMIP deposition data and the fertilizer data[34] were selected as the nitrogen inputs for our attribution analysis experiment (Fig. 1b and Supplementary Table 2) and model calibration (Supplementary Figs. 3–6). The historical global gross domestic product and population data obtained from the intersectoral impact model intercomparison project (ISIMIP, https://esg.pik-potsdam.de/search/isimip/) are used for estimating sewage N exports, using the method proposed by Van Drecht et al.[38].

Uncertainty analysis. We have evaluated three main sources of uncertainty in estimating riverine N_2O emissions: (1) N input data-induced uncertainty, (2) river surface area-induced uncertainty and (3) parameter-induced uncertainty. To evaluate uncertainty of riverine N_2O emissions induced by nitrogen input data, we carried out four simulations by using different nitrogen input datasets. We first chose ACCMIP deposition[32] data and fertilizer data[34] as a benchmark and then substituted N fertilizer data with datasets[35,36] for two other separate experiments. We also replaced ACCMIP N deposition data with CCMI N deposition data[33] for running another simulation.

Moreover, we quantified uncertainty induced by different estimates of river surface area (Supplementary Information). Since uncertainty in river surface area estimates mainly originated from the headwater zones[22], we implemented an uncertainty analysis for the river shape parameter (r) to represent the global river surface areas 0.77, 0.71, 0.52, 0.41 and 0.34 ($\times 10^6$ km^2), which aligns well with several previous estimates of global total river surface area[23,39,40]. The temporal trends of riverine N_2O emissions with uncertainty ranges can be seen in Supplementary Fig. 7.

We performed sensitivity analysis and four key parameters for riverine N_2O emissions were identified. The valid ranges of the four parameters were determined according to previous literature (Supplementary Information). Specifically, $k_{g/h}$ (ratio of groundwater N_2O production from NO_3^- leaching rate) varied from 0.33% to 1.63% (ref. [41]), $k_{reduction}$ (N_2O consumption rate) varied from 0.0057 to 0.0344 (Supplementary Table 5) and $R_{denitrif}$ and R_{nitrif} (ratios of riverine N_2O production from riverine denitrification and nitrification, respectively) varied from 0.3% to 3% (ref. [8]), consistent with the uncertainty analysis in a most recent modelling study[8]. The Latin hypercube sampling approach was applied to randomly generate 50 sets of parameters from the high-dimension parameter space[42,43] (through MATLAB R2017a). We conducted 50 model simulations for 1900 to 2016 keeping all drivers consistent with factorial analysis. The mean riverine N_2O emissions of the 50 simulations are shown in Supplementary Fig. 5 with uncertainty range of ±1 s.d.

Theoretically, uncertainties from model parameters and input data are independent from each other, and thus their joint uncertainty was calculated as the square root of the quadratic sum of the three uncertainties[44].

Data availability

The relevant datasets of this study are archived in the box site of International Center for Climate and Global Change Research at Auburn University (https://auburn.box.com/v/GriverineN2O). Source data for Figs. 1–4 and Supplementary Figs. 1–10 are provided with the paper.

Code availability

The relevant code of this study is available from the corresponding author on request.

References

31. Jung, M., Henkel, K., Herold, M. & Churkina, G. Exploiting synergies of global land cover products for carbon cycle modeling. *Remote Sens. Environ.* **101**, 534–553 (2006).
32. Lamarque, J.-F. et al. The atmospheric chemistry and climate model intercomparison project (ACCMIP): overview and description of models, simulations and climate diagnostics. *Geosci. Model Dev.* **6**, 179–206 (2013).
33. Eyring, V. et al. *Overview of IGAC/SPARC Chemistry–Climate Model Initiative (CCMI) Community Simulations in Support of Upcoming Ozone and Climate Assessments* SPARC Newsletter No. 40 (WMO-WCRP, 2013).
34. Lu, C. & Tian, H. Global nitrogen and phosphorus fertilizer use for agriculture production in the past half century: shifted hot spots and nutrient imbalance. *Earth Syst. Sci. Data* **9**, 181–192 (2017).
35. Nishina, K., Ito, A., Hanasaki, N. & Hayashi, S. Reconstruction of spatially detailed global map of NH_4^+ and NO_3^- application in synthetic nitrogen fertilizer. *Earth Syst. Sci. Data* **9**, 149–162 (2017).
36. Zaehle, S., Ciais, P., Friend, A. D. & Prieur, V. Carbon benefits of anthropogenic reactive nitrogen offset by nitrous oxide emissions. *Nat. Geosci.* **4**, 601 (2011).
37. Zhang, B. et al. Global manure nitrogen production and application in cropland during 1860–2014: a 5 arcmin gridded global dataset for Earth system modeling. *Earth Syst. Sci. Data* **9**, 667–678 (2017).
38. Van Drecht, G., Bouwman, A. F., Harrison, J. & Knoop, J. M. Global nitrogen and phosphate in urban wastewater for the period 1970 to 2050. *Glob. Biogeochem. Cycles* **23**, GB0A03 (2009).
39. Allen, G. H. & Pavelsky, T. M. Global extent of rivers and streams. *Science* **361**, 585–588 (2018).
40. Bastviken, D., Tranvik, L. J., Downing, J. A., Crill, P. M. & Enrich-Prast, A. Freshwater methane emissions offset the continental carbon sink. *Science* **331**, 50–50 (2011).
41. Jahangir, M. M. et al. Groundwater: a pathway for terrestrial C and N losses and indirect greenhouse gas emissions. *Agric. Ecosyst. Environ.* **159**, 40–48 (2012).
42. Tian, H. et al. Global methane and nitrous oxide emissions from terrestrial ecosystems due to multiple environmental changes. *Ecosyst. Health Sustain.* **1**, 1–20 (2015).
43. Tian, H. et al. Net exchanges of CO_2, CH_4, and N_2O between China's terrestrial ecosystems and the atmosphere and their contributions to global climate warming. *J. Geophys. Res. Biogeosci.* **116**, G02011 (2011).
44. Heuvelink, G. B. *Error Propagation in Environmental Modelling with GIS* (CRC, 1998).

Acknowledgements

This research was made possible partly by NSF grant nos. 1903722 and 1243232; NASA grant nos. NNX14AO73G, NNX10AU06G, NNX11AD47G and NNX14AF93G; NOAA grant nos. NA16NOS4780207 and NA16NOS4780204; Ocean University of China-Auburn University Joint Progam; and Andrew Carnegie Fellowship Award no. G-F-19-56910. The statements made and views expressed are solely the responsibility of the authors.

Author contributions

H.T. initiated and designed this research. Y.Y. improved and developed the model and implemented simulation experiments. H.S. and R.X. contributed to result analysis and

interpretation. N.P. gave technical support to implement simulation experiments and uncertainty analysis. J.G.C., S.P. and all other authors contributed to the writing and development of the manuscript.

Competing interests

The authors declare no competing interests.

Additional information

Supplementary information is available for this paper at https://doi.org/10.1038/s41558-019-0665-8.

Correspondence and requests for materials should be addressed to H.T.